Multiple Shear-Banding Transitions in a Supramolecular Polymer Solution

J. van der Gucht,[1,*] M. Lemmers,[1] W. Knoben,[1] N. A. M. Besseling,[1] and M. P. Lettinga[2]

[1]*Laboratory of Physical Chemistry and Colloid Science, Wageningen University, PO Box 8038, 6700 EK Wageningen, The Netherlands*

[2]*Forschungszentrum Jülich, IFF, Weiche Materie, 52425, Jülich, Germany*

(Received 6 June 2006; published 7 September 2006)

We report on the nonlinear rheology of a reversible supramolecular polymer based on hydrogen bonding. The coupling between the flow-induced chain alignment and breakage and recombination of bonds between monomers leads to a very unusual flow behavior. Measured velocity profiles indicate three different shear-banding regimes upon increasing shear rate, each with different characteristics. While the first of these regimes has features of a mechanical instability, the second shear-banding regime is related to a shear-induced phase separation and the appearance of birefringent textures. The shear-induced phase itself becomes unstable at very high shear rates, giving rise to a third banding regime.

DOI: 10.1103/PhysRevLett.97.108301 PACS numbers: 83.60.Rs, 47.50.−d, 83.60.Wc, 83.80.Rs

Coupling between fluid microstucture and flow yields a rich scala of non-Newtonian behavior in complex fluids. Many complex fluids display flow instabilities or flow-induced phase transitions above a critical shear rate or stress. Solutions of wormlike micelles, for example, undergo a shear-banding instability in which the fluid separates in the gradient direction into coexisting regions (bands) supporting different shear rates (''gradient banding'') [1,2]. Rod-like colloids, on the other hand, display ''vorticity banding,'' in which the different shear bands are separated in the vorticity direction [3]. Several other systems, such as attractive emulsions or carbon nanotube suspensions, show an elastic instability that leads to the formation of shear-induced aggregates aligned in the vorticity direction [4,5].

Several aspects of these instabilities can be reproduced by phenomenological models, see e.g. [6]. Shear banding in the gradient direction, for example, can be related to a nonmonotonic constitutive equation relating the shear stress σ and the shear rate $\dot{\gamma}$. When a shear rate is applied in the region where σ decreases with $\dot{\gamma}$, an initially homogeneous flow becomes mechanically unstable. In the simplest scenario, the system then separates into a weakly sheared band that flows at $\dot{\gamma}_1$ and a highly sheared band that flows at $\dot{\gamma}_2$ [1]. Increasing the overall shear rate within the unstable region leads to an increase of the width of the high shear band, while the stress remains constant. The microscopic origin of the shear-banding instability varies for different systems. For wormlike micelles, two alternative mechanisms for shear banding have been proposed. Cates and coworkers predicted a nonmonotonic constitutive equation leading to a shear-banding instability, based on the Doi and Edwards reptation model for polymers [1]. This purely mechanical instability is responsible for shear banding in semidilute solutions of wormlike micelles, far from an equilibrium phase transition [2]. In more concentrated systems, on the other hand, the appearance of a banded flow is related to a first-order phase transition induced by the flow, such as an isotropic-to-nematic transition [6,7]. In this case, the two shear bands correspond to two structurally different coexisting phases.

Most experimental studies on shear banding have been performed with solutions of wormlike micelles. These have been successfully described as reversible equilibrium polymers that can break and recombine on experimental timescales [8]. In recent years, various other types of reversible supramolecular polymers have been synthesized, based on more specific reversible interactions, such as metal coordination complexes and hydrogen bonding [9]. The availability of these polymers paves the way for experiments that will lead to a more general understanding of the flow behavior of reversible polymers.

In this Letter, we report for the first time on shear banding in a solution of reversible supramolecular polymers based on hydrogen bonding. The unique feature of this system is that we observe *three* different shear-banding regimes upon variation of the shear rate, each with different characteristics. While the banded state at low shear rates has features of a mechanical instability, the second shear-banding regime is related to a shear-induced phase transition and the appearance of texture. In this region, we find a very unusual relation between the relative widths of the two shear bands and the overall shear rate: the width of the high-shear band *decreases* when the global shear rate increases. At very high shear rates, the shear-induced phase becomes itself unstable, giving rise to a third banding regime.

The system under examination is a solution of bis-urea-substituted toluene (EHUT), a bifunctional monomer that assembles reversibly into long, semiflexible polymer chains by multiple hydrogen bonds [10]. The persistence length of EHUT polymers was estimated to be at least 100 nm [11], which is an order of magnitude larger than for most wormlike micelles [8]. We study solutions of EHUT in dodecane at concentrations up to 6.4 g/l at 20 °C. No evidence for an isotropic-to-nematic phase tran-

sition (at rest) was observed for this concentration range and temperature. Rheological measurements were performed on a Paar Physica MCR 300 rheometer in controlled strain mode using a Couette geometry of 26.66 mm inner diameter and 1.13 mm gap width and a solvent trap to minimize evaporation. It was checked that a different Couette geometry gave only small differences. Spatially resolved velocity profiles were measured in a closed transparent Couette cell (43 mm inner diameter, 2.5 mm gap) using heterodyne dynamic light scattering in combination with a differential Laser Doppler velocimeter [12]. The rheo-optical properties of the sheared solutions were studied by placing a transparent Couette cell (43 mm inner diameter, 2.5 mm gap) between crossed polarizers. Images were taken in the plane defined by the flow and vorticity directions so that the measured birefringence is an average over the gap.

Figure 1 shows the steady state shear stress σ as a function of the shear rate $\dot{\gamma}$ for a 5.9 g/l EHUT solution at 20 °C. Several regimes are indicated in this figure. In regime A ($\dot{\gamma} < \dot{\gamma}_I \approx 0.01\ s^{-1}$), the stress increases linearly with the shear rate. The solution behaves as a Maxwell fluid in this regime with a viscosity η of 368 Pa · s, plateau modulus G_0 of 16 Pa and a relaxation time τ_0 of 23 s as obtained from the transient stress response after startup of shear flow and from dynamic linear rheology measurements. At $\dot{\gamma} = \dot{\gamma}_I \approx 0.01\ s^{-1}$ and $\sigma = \sigma_B \approx 3.3$ Pa, there is an abrupt change of slope, after which the stress decreases slightly with increasing shear rate. After reaching a minimum, the stress increases again, but with a much lower slope than in the linear regime. Region B is characterized by stress overshoots, very slow transient behavior

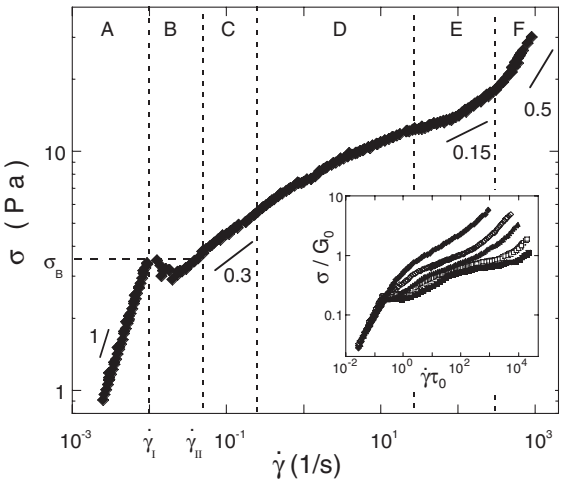

FIG. 1. Shear stress as a function of shear rate for a 5.9 g/l EHUT solution at 20 °C (measured under controlled shear rate). A–F indicate different flow regimes. In regimes B, D, and E, a banded flow is observed. Inset: flow curves for EHUT concentrations of 1.4 (◆), 2.0 (◇), 3.1 (▲), 5.9 (□), and 6.4 (■) g/l; $\dot{\gamma}$ is normalized by the terminal relaxation time τ_0 and σ is normalized by the plateau modulus G_0.

(it may take hours before a steady state is reached), and metastability. At $\dot{\gamma} > \dot{\gamma}_{II} \approx 0.06\ s^{-1}$, the stress exceeds σ_B and increases with increasing shear rate with a slope of about 0.3 (regime C). In regime D, the slope of the flow curve decreases and reaches a minimum of around 0.08 at $\dot{\gamma} \simeq 30\ s^{-1}$. In regime E, the slope increases again, and it eventually reaches a value of around 0.5 in regime F. Regimes D and E are again characterized by slow transient behavior. Care was taken to ensure that the points in Fig. 1 really correspond to the steady state values for the stress. Different shear histories were applied to the solution, which all resulted in the same steady state value. We also measured a flow curve in controlled stress mode. This gave the same result, except that no points could be measured in regime B: at $\sigma = \sigma_B$, the shear rate "jumps" from $\dot{\gamma}_I$ to $\dot{\gamma}_{II}$. As indicated in the inset in Fig. 1, flow curves at different concentrations exhibit qualitatively the same characteristics. The onset of regime B occurs at the same normalized shear rate $\dot{\gamma}_I \tau_0 = 0.20 \pm 0.03$ and stress $\sigma_B/G_0 = 0.18 \pm 0.03$ for all concentrations, where G_0 and τ_0 both increase with increasing concentration [11]. At higher shear rates, the normalized flow curves do not superimpose, and the normalized stress at a certain normalized shear rate decreases with increasing concentration.

Figure 2 shows velocity profiles in the gap of the Couette cell measured at different applied overall shear rates. The lowest shear rate for which a velocity profile could be

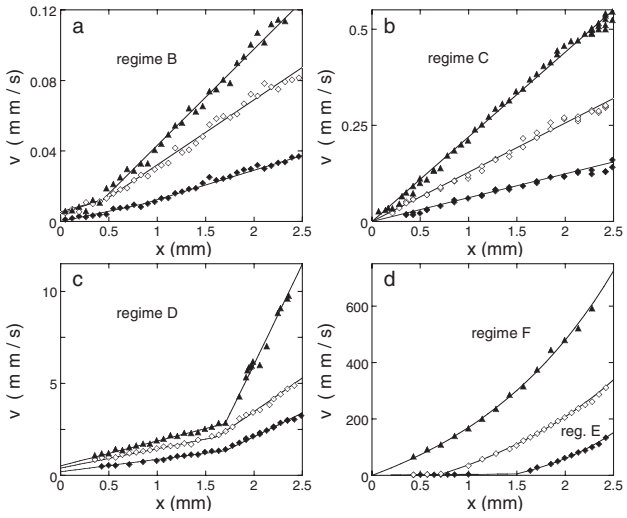

FIG. 2. Velocity profiles in the Couette cell at different applied shear rates $\dot{\gamma}$. (a) Regime B, $\dot{\gamma} = 0.015$ (◆), $\dot{\gamma} = 0.025$ (◇), and $\dot{\gamma} = 0.05$ (▲) s^{-1}. Drawn lines are linear fits for both bands. (b) Regime C, $\dot{\gamma} = 0.066$ (◆), $\dot{\gamma} = 0.14$ (◇), and $\dot{\gamma} = 0.23$ (▲) s^{-1}. Drawn lines corresponds to $v = \dot{\gamma}x$. (c) Regime D, $\dot{\gamma} = 0.59$ (◆), $\dot{\gamma} = 1.5$ (◇), and $\dot{\gamma} = 4.9$ (▲) s^{-1}. Lines are linear fits for both bands. (d) Regime E, $\dot{\gamma} = 64$ (◆) and $\dot{\gamma} = 147$ (◇) s^{-1}, and beginning of regime F, $\dot{\gamma} = 308\ s^{-1}$ (▲). Drawn lines correspond to a linear profile for the low shear band and a power-law fluid ($\sigma \sim \dot{\gamma}^{0.15\pm0.02}$) for the high shear band. No slip was observed at the moving wall in all cases.

measured was 0.01 s^{-1}, just on the boundary of regimes *A* and *B*. The velocity profile is linear, as expected for a Newtonian solution. At shear rates between 0.015 and 0.066 s^{-1} (regime *B*, Fig. 2(a)], the profiles exhibit a "kink" indicating a banded structure. The kink becomes more pronounced with increasing shear rate. The measured velocity profiles also enable a quantification of wall slip. In regime *B*, there is a marginal slip at the stationary outer cylinder. At shear rates between 0.066 and 0.25 s^{-1} (regime *C*, Fig. 2(b)), the profiles are linear, indicating that the flow is homogeneous. Slip is negligible in this regime. An unambiguous banded state is observed again in regimes *D* and *E*, at shear rates between 0.25 and 300 s^{-1}. In regime *D*, between 0.25 and 30 s^{-1}, the velocity profile in both shear bands is approximately linear [Fig. 2(c)], while in regime *E*, above 30 s^{-1}, the high-shear band has a strongly curved profile [Fig. 2(d)]. At the highest shear rate applied ($\dot{\gamma} = 308\ s^{-1}$), the low shear band has disappeared and only one band is left, also with a curved velocity profile (regime *F*, Fig. 2(d)]. The curved velocity profiles in regimes *E* and *F* are an indication for strong shear thinning in these regimes [12]. The profile for $\dot{\gamma} = 308\ s^{-1}$ can be fitted with a power-law fluid $\sigma \sim \dot{\gamma}^a$ with an exponent $a = 0.15$ [13]. The same shear-thinning exponent accounts for the profiles in the high shear band in regime *E*. A slope of 0.15 is also indicated in the flow curve shown in Fig. 1. It can be seen in this figure that this exponent is in reasonable agreement with the slope of the measured flow curve in the relevant region (regime *E* and the beginning of regime *F*).

Solutions of EHUT thus exhibit *three* different shear-banding regimes. The onset of the first shear-banding regime (*B*) occurs at the same normalized shear rate $\dot{\gamma}_1\tau_0$ and stress σ_B/G_0 for different EHUT concentrations (Fig. 1, inset), suggesting that the origin of shear banding in this regime is a mechanical instability of the underlying constitutive relation, such as proposed by Spenley and Cates [1]. Indeed, birefringence images show no evidence for a shear-induced phase transition in regime *B* [Fig. 3(a)]: no significant increase of the birefringence could be detected in regimes *B* and *C*. The unstable flow behavior is also supported by the jump in the flow curve when measured under controlled stress. The shear-banded flow at higher shear rates, in regimes *D* and *E*, on the other hand, is accompanied by the appearance of birefringent textures in the solution [Fig. 3(b)–3(d)]. These textures could be seen for the first time at a shear rate of about 1 s^{-1} (i.e. in regime *D*). They appear a few seconds after startup of shear flow and remain visible for many hours under steady flow. After cessation of the shear flow, the textures disappear again on the timescale of several seconds. With increasing shear rate, the overall birefringence increases and the textures become finer and at very high shear rates, they seem to disappear [Fig. 3(d)]. Without polarized incoming light, no texture could be seen. The textures can be interpreted as domains of a new phase induced by the shear flow and suggest that, contrary to regime *B*, the banded structure in regimes *D* and *E* is related to a shear-induced phase separation (for example between an isotropic and a nematic phase). Similar domain patterns have been seen in other multiphase flows where they were attributed to a viscoelastic asymmetry between the two phases [5]. In wormlike micelle solutions, a shear-induced phase transition is observed only for very concentrated micellar solutions, close to an equilibrium phase transition [7]. For EHUT solutions, we did not see evidence for a phase transition at rest for the concentrations used, but, nevertheless, a transition is induced by the flow. This suggests that the flow couples more strongly to chain alignment and growth for EHUT than for wormlike micelles, probably because of the longer persistence length of EHUT polymers [8,11].

In order to obtain more detailed information about the behavior in the three different shear-banding regimes, we extract from the velocity profiles displayed in Fig. 2 the average shear rates in both shear bands and the width of the two bands. These are shown in Fig. 4 as a function of the overall applied shear rate. Clearly, our observations do not correspond to the simple picture in which a change of the applied shear rate only affects the relative proportion of

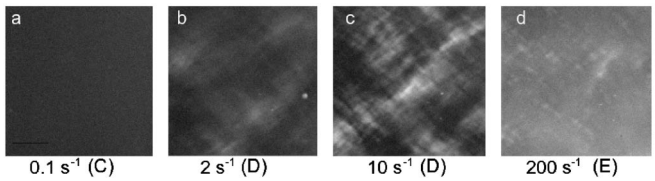

FIG. 3. Birefringence images taken in the plane defined by the flow and vorticity directions of a 5.9 g/l EHUT solution at 20 °C under shear flow for different applied shear rates (as indicated). The flow regime is indicated in parentheses. Each image is 1 × 1 cm.

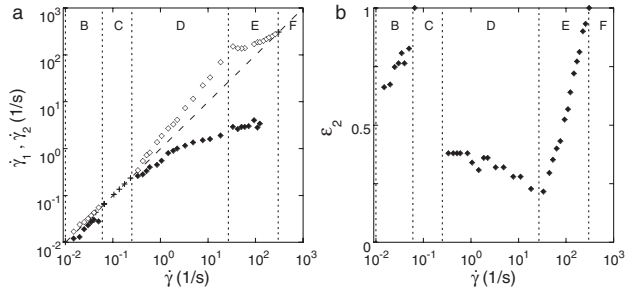

FIG. 4. (a) Average shear rates $\dot{\gamma}_1$ in the low shear band (◆) and $\dot{\gamma}_2$ in the high shear band (◇) as a function of the overall shear rate. + indicates shear rates in regime *C*, where no shear-banding is observed. The diagonal dashed line denotes homogeneous flow. (b) Fraction ε_2 of the gap occupied by the high shear band as a function of the overall shear rate. Note that there is only one band in regimes *A*, *C*, and *F*. Vertical dashed lines in both figures indicate different regimes *A*–*F*.

each layer, while the shear rates in both bands and the value of the stress remain constant [1]. In regime B, we find that both the shear rate in the low shear band $\dot{\gamma}_1$ and that in the high shear band $\dot{\gamma}_2$ increase with increasing $\dot{\gamma}$. Moreover, we do not see a clear stress plateau in the flow curve (Fig. 1). These observations may be due to the inherent stress gradient of the Couette cell. Alternatively, the compositions of the two bands could be different and vary when the overall shear rate is varied [6]. The relative width of the high shear band ϵ_2 increases with the overall shear rate $\dot{\gamma}$ in regime B, as expected [1]. It approaches unity as regime C is approached, where the banded structure disappears. The difference in viscosity between the two bands in regime B is rather small: the ratio $\dot{\gamma}_2/\dot{\gamma}_1$ varies between 1 and 2. In regime D, where shear banding is related to a phase transition (as seen from birefringence images), the variation of $\dot{\gamma}_1$, $\dot{\gamma}_2$, and ϵ_2 with $\dot{\gamma}$ is rather unusual. Upon increasing the shear rate, ϵ_2 first remains more or less constant and then *decreases*, while the ratio between the shear rates in both bands ($\dot{\gamma}_2/\dot{\gamma}_1$) increases from 1 to approximately 50. Clearly, such behavior cannot be explained by current theory. It suggests a complex interplay between the structure of the two phases, the concentrations and length distributions in both phases, and the shear flow. In regime E, the behavior is more or less as expected. Upon increasing the overall shear rate, the shear rates in the two bands remain approximately constant, while ϵ_2 increases monotonically to unity at the boundary between regimes E and F, where also the textures disappear. The behavior of $\dot{\gamma}_1$, $\dot{\gamma}_2$, and ϵ_2 upon variation of the overall shear rate changes very abruptly at $\dot{\gamma} \approx 30\ \mathrm{s}^{-1}$, between regimes D and E. As noted above, the shapes of the velocity profiles also change here: in regime D the profiles are linear in both bands, while in regime E the high shear band is strongly curved [Fig. 2(c) and 2(d)]. These observations suggest that the shear-induced phase that is formed in regime D becomes unstable in regime E, thus giving rise to a third shear-banding regime. Whether this instability is a mechanical instability or a phase transition to a new shear-induced phase or structure is unclear. It would be useful to extend the present rheological study with scattering techniques, microscopy, or birefringence imaging in the vorticity direction to obtain information about the microstructure of the two phases.

In summary, we studied the nonlinear rheology of a solution of hydrogen-bonded supramolecular equilibrium polymers. Upon variation of the shear rate, these polymers exhibit a very rich and complex behavior with three different shear-banding regimes. For the first time, we observe within the same system the two different types of gradient shear banding that have been described: a mechanical instability at low shear rates and a shear-induced phase transition at higher shear rates. The characteristics of the banded flow regimes cannot be fully explained by current theories and ask for a detailed microscopic modeling of equilibrium polymers under flow that takes into account the coupling between flow alignment, reversible breakage and recombination reactions, and concentration gradients in the gap. By comparing with other types of reversible supramolecular polymers and contrasting to wormlike micelles, we may be able to extract the role of specific bonding interactions and chain flexibility in these systems. Alternatively, by adding monofunctional monomers that block chain ends and prevent their recombination [14], one could investigate the role of recombination reactions, while adding trifunctional monomers would give the possibility of bundle or network formation.

The authors thank L. Bouteiller for supplying EHUT samples and H. Kriegs for assistance with the heterodyne light scattering measurements.

*Electronic address: jasper.vandergucht@wur.nl

[1] N. A. Spenley, M. E. Cates, and T. C. B. McLeish, Phys. Rev. Lett. **71**, 939 (1993).
[2] H. Rehage and H. Hoffmann, Mol. Phys. **74**, 933 (1991).
[3] M. P. Lettinga and J. K. G. Dhont, J. Phys. Condens. Matter **16**, S3929 (2004).
[4] A. Montesi, A. Peña, and M. Pasquali, Phys. Rev. Lett. **92**, 058303 (2004).
[5] E. K. Hobbie, S. Lin-gibson, H. Wang, J. A. Pathak, and H. Kim, Phys. Rev. E **69**, 061503 (2004).
[6] S. M. Fielding and P. D. Olmsted, Eur. Phys. J. E **11**, 65 (2003).
[7] J. F. Berret, D. C. Roux, and P. Lindner, Eur. Phys. J. B **5**, 67 (1998).
[8] M. E. Cates and S. J. Candau, J. Phys. Condens. Matter **2**, 6869 (1990).
[9] L. Brunsveld, B. J. B. Folmer, E. W. Meijer, and R. P. Sijbesma, Chem. Rev. **101**, 4071 (2001).
[10] S. Boileau, L. Bouteiller, F. Lauprêtre, and F. Lortie, New Journal of Chemistry **24**, 845 (2000).
[11] J. Van der Gucht, N. A. M. Besseling, W. Knoben, L. Bouteiller, and M. A. Cohen Stuart, Phys. Rev. E **67**, 051106 (2003).
[12] J.-B. Salmon, A. Colin, and S. Manneville, Phys. Rev. Lett. **90**, 228303 (2003).
[13] The velocity profile for a power law fluid with $\sigma \sim \dot{\gamma}^a$ in a Couette geometry is $v(r) = \omega_0 r(r^{-2/a} - R_2^{-2/a})/(R_1^{-2/a} - R_2^{-2/a})$, with ω_0 the applied angular velocity, R_1 the radius of the inner cylinder, R_2 that of the outer cylinder, and $r = R_2 - x$ the distance from the center of the cylinders [12].
[14] W. Knoben, N. A. M. Besseling, L. Bouteiller, and M. A. Cohen Stuart, Phys. Chem. Chem. Phys. **7**, 2390 (2005).